Electronic Supplementary Information

Solvothermal-Assisted Synthesis for Self-Assembling TiO_2 Nanorods on Large Graphitic Carbon Nitride Sheets with Their Anti-Recombination in Photocatalytic Removal of Cr(VI) and Rhodamin B Under Visible Light Irradiation

Dingze Lu[†], Pengfei Fang*[,†], Wenhui Wu[†], Junqian Ding[†], Lulu Jiang[†], Xiaona Zhao[†], Chunhe Li[†], Minchen Yang[†] and Yuanzhi Li[‡]

[†]Department of Physics and Key Laboratory of Artificial Micro– and Nano–structures of Ministry of Education, Wuhan University, Wuhan 430072, P.R. China

*,[†]Corresponding author: Pengfei Fang
Tel : +86 27 6875 2003;
Fax: +86 27 6875 2003;
E–mail address: fangpf@whu.edu.cn (Pengfei Fang).

[‡]State Key Laboratory of Silicate Materials for Architectures, Wuhan University of Technology, 122 Luoshi Road, Wuhan 430070, P.R. China

****

Experimental Section

Degussa P25 (TiO_2, 80% anatase, 20% rutile) is the product of Degussa Co., Ltd. The sodium hydroxide (NaOH), acetone (C_3H_6O), *tert*-butyl alcohol (TBA), urea ($CO(CH_2)_2$), phosphoric acid (H_3PO_4), 1, 5–Diphenylcarbohydrazide ($C_{13}H_{14}N_4O$), ethyl alcohol (C_2H_5OH), hydrogen peroxide (H_2O_2), Rhodamin B (RhB), and potassium dichromate ($K_2Cr_2O_7$) were provided by Sinopharm Chemical Reagent Co., Ltd, and coumarin was obtained from Alfa Aesar.

Evaluation of photocatalytic activity for dichromate ($K_2Cr_2O_7$) solution

The photocatalytic reduction of aqueous Cr(VI) to Cr(III) was performed at 25 °C ± 2 °C in a 200 mL of quartz reactor containing 100 mg of photocatalyst and 100 mL of Cr(VI) aqueous solution at a concentration of 50 ppm. The pH values of solutions were adjusted with HCl or NaOH. Without any additives, the pH value of the suspension was found to be at around 6.8. Adsorption was monitored in the darkness during the periodically withdrawing a small amount of solution (0.2 mL) provided a continuous dilution, complexing, and measurement. Once the adsorption-desorption equilibrium is reached, the reactor was exposed to a 300 W Xe lamp (172 mW/cm^2, 15 cm away from the photocatalytic reactor). The total duration of the reaction process was 70 min under constant air-equilibrated conditions during the irradiation. For every 10 min, 0.8 mL of solution was collected and centrifuged for 2 min to separate the photocatalyst at a speed of 12,000 r/min. The final samples were obtained by 0.4 mL of supernatant liquor mixed with 2.8 mL of deionized water water. The Cr(VI) content in the supernatant solution was analyzed colorimetrically at 540 nm using the diphenylcarbazide method (DPC) by UV-vis spectrometer. The visible-light photocatalytic activity was evaluated, using a cut-off filter ($\lambda \geq 420$ nm).

Evaluation of photocatalytic activity of samples for RhB

The photocatalytic activities of samples were evaluated by the degradation of RhB solution with the same light source and the photocatalytic reactor. In photocatalytic reaction, the suspensions of the reaction were obtained by adding 0.1 g of photocatalyst into 100 mL of 20 mg/L RhB solution. The reaction apparatus were put into water bath to maintain at ambient temperature. Similarly, the Xe lamp was turned on after stirring the solution in darkness for 1 h to make sure that the adsorption-desorption equilibrium has been established before the photocatalytic reaction. The whole reaction process lasted 70 min. Every 10 min, 1.6 mL of solution was collected and centrifuged to separate the photocatalyst with a speed of 12,000 r/min for 2 min. The final testing samples were obtained by 0.8 mL of supernatant liquor mixed with 2.4 mL of deionized water. The concentrations of RhB solution were determined by the UV-vis spectrometer. Blank experiment was carried out without any photocatalysts to test the stability of RhB molecules. When the visible-light photocatalytic reaction was performed, a cut-off filter ($\lambda \geq 420$ nm) was put on the top of the apparatus of the reaction.

Evaluation of adsorption capacity of samples for RhB

The samples' adsorption capacity for RhB was evaluated. In the adsorption process, 0.1 g catalyst was added into 100 mL of RhB aqueous RhB solution (20 mg/L). The suspensions were stirred for 1 h in dark to reach adsorption-desorption equilibrium. Once reaching the adsorption-desorption equilibrium, 1.6 mL of solution was collected and centrifuged for 2 min at a speed of 12,000 r/min to separate the photocatalyst. The final samples were obtained by 0.8 mL of supernatant liquor mixed with 2.4 mL of deionized water. The RhB content in the supernatant solution was analyzed colorimetrically at 554 nm by UV-vis spectrometer. The adsorption capacity η (%) of catalyst was calculated by the following equation η (%) = $[(C_i–C_e)/ C_i]\times100\%$, where C_i is initial concentration, and C_e is equilibrium concentration of RhB solution.

Surface photocurrent (SPC), Linear sweep voltammetry (LSV) spectra, electrochemical impedance spectra (EIS), and Tafel spectra experiments

Initially, 5 mg of TNSs, g-C_3N_4, or TNRs/g-C_3N_4 samples were dispersed in 5 mL of ethanol, respectively. After 90 min of sonication, the slurries were dip-coated onto an indium-tin oxide (ITO) glass electrode (1 × 2 cm) and then dried under infrared light. During the investigations, the as-prepared photocatalyst/ITO electrodes, the saturated calomel electrode, and platinum electrode were employed as the working electrode, reference electrode and counter electrode, respectively. Na_2SO_4 aqueous solution with the concentration at 1 M was chosen as electrolyte. The working electrode (the prepared photocatalyst/ITO electrodes) was irradiated horizontally by a high-pressure Xe lamp (300 W) equipped with a cut-off filter ($\lambda \geq 420$ nm) that is kept at 15 cm apart. The surface photocurrent (SPC) tests in the present experiments were performed by the electrochemical workstation (CHI-660C, Chenhua, China). Similarly, the electrochemical impedance spectra (EIS) were also measured by the same electrochemical system (CHI-660C, Chenhua, China). Na_2S solution (0.1 M) was used as the electrolyte solution. However, the linear sweep voltammetry (LSV) spectra and Tafel experiments were obtained by the saturated Ag/AgCl electrode being employed as the reference electrode. The electrolyte including 0.1 M of Na_2SO_4 aqueous solution (80 mL) and 20 mL of ethanol was employed. The tests also were carried out by the same electrochemical workstation.

Analysis of photo-generated hydroxyl radicals (•OH)

The formation of •OH radicals on the illuminated photocatalysts was analyzed by the photoluminescence (PL) technique using coumarin (COU) as a probe molecule. COU can readily react with •OH to form highly fluorescent COU-OH adducts (7-hydroxycoumarin). The intensity of

PL of 7-hydroxycoumarin (7-HC) was proportional to the amount of •OH radicals formed on the surface of the photocatalysts.[S1-S2] The visible-light irradiation was obtained by the same cut-off filter. The suspensions were carried out by adding photocatalyst (0.2 g) into aqueous COU solution (1 mM, 100 mL). After achieving adsorption-desorption equilibrium by magnetic stirring in dark for 1 h, the suspensions containing COU as well as photocatalyst powder were irradiated by 300 W Xe lamps under constant air-equilibrated conditions. PL spectra of 7-HC product were detected once every 5 min on a fluorescence spectrophotometer (Hitachi F-4600). The increase in the PL intensity at 450 nm of 7-HC by excitation with a wavelength of 342 nm was measured.

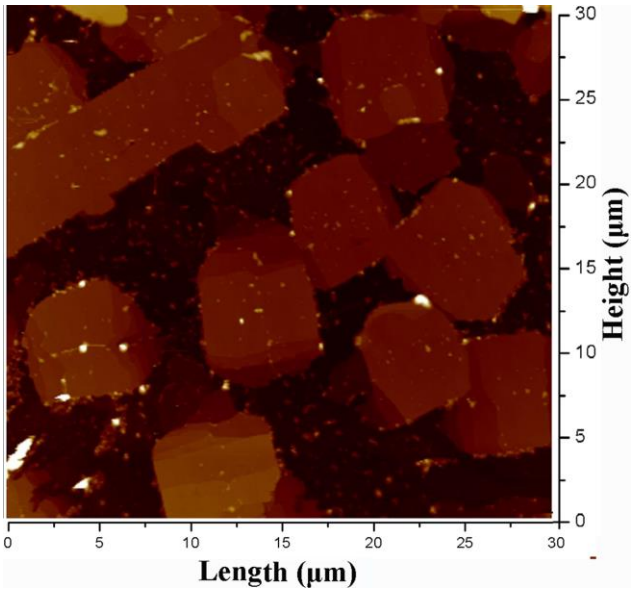

Fig. S1. AFM image of g-C_3N_4 as-prepared nanosheets.

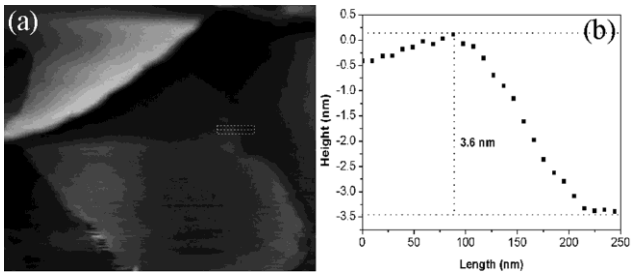

Fig. S2. (a) AFM images of pure TiO_2-based nanosheets; (b) line profile showing the height of TiO_2-based nanosheets.

Atomic force microscopy (AFM) was utilized to analyze the surface morphology and thickness of TiO_2-based nanosheets (TNSs). As shown in Fig. S2, it can be also found that TNSs possess a large surface size (ca. 1–3 μm) which is far larger than the size of unexfoliated nanoparticles (20–40 nm), and small thickness (ca. 3.6 nm) which is much thinner than that of the raw TiO_2 nanoparticles. Besides, the g-C_3N_4 samples display clearly sheet-like structure with large surface areas. Both large

surface sizes are beneficial to the connection between TNSs and g-C_3N_4, and small thickness of TNSs made the splitting of TNSs easier and formation of TiO_2-based nanorods (TNRs) more convenient in the solvothermal reaction.

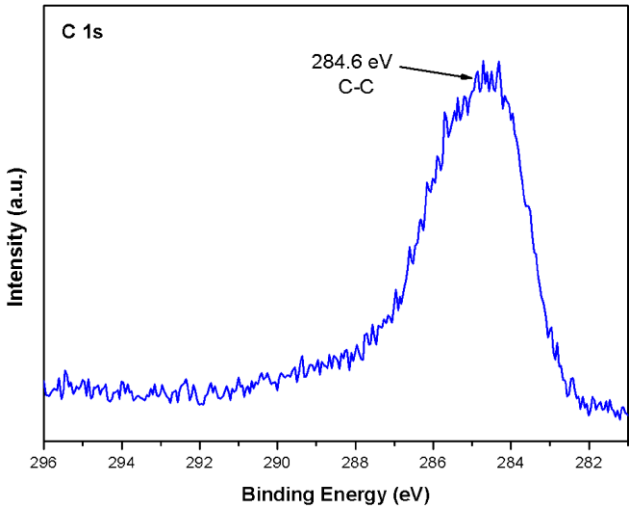

Fig. S3. XPS spectra of C 1s region for TNRs samples (The carbon is derived from carbon contamination for standardizing).

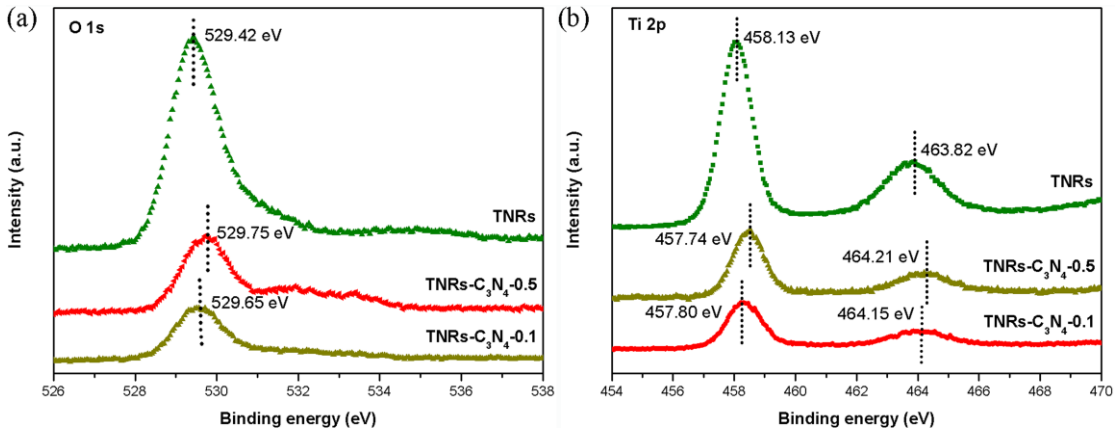

Fig. S4. XPS spectra O 1s region (a) and Ti 2p region (b) of TNRs, TNRs-C_3N_4-0.1, and TNRs-C_3N_4-0.5.

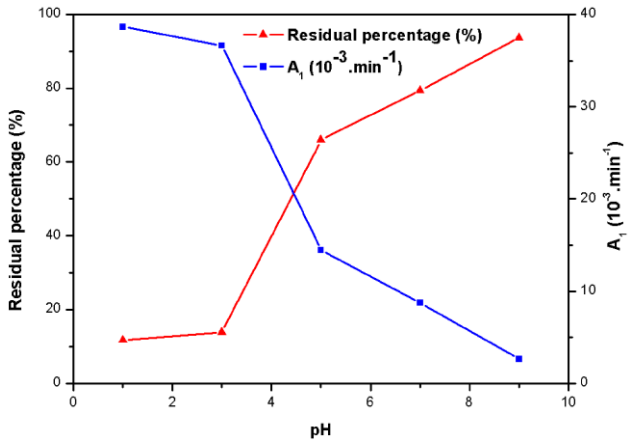

Fig. S5. Photocatalytic reduction of Cr(VI) and the reaction rate constant (A_1) at different pH for TNRs-C_3N_4-0.1 under visible light irradiation. Initial concentration of Cr(VI) was 50 ppm, and the dosage of TNRs-C_3N_4-0.1 was 1 g/L.

Fig. S5 shows visible-light photocatalytic reduction of Cr(VI) and the reaction rate at different pH for TNRs-C_3N_4-0.1. It is well-known that photocatalytic reduction of Cr(VI) primarily depend on pH values.[S3,S4] It can be found that the decrease of pH would strongly promote photocatalytic reduction of Cr(VI), and the maximum reaction rate reached $12.069\times10^{-3}\cdot min^{-1}$ at pH 1, while the reaction rate was $1.27\times10^{-3}\cdot min^{-1}$ for the pH value 9. Low pH values attributed the main species Cr(VI) of $H_2Cr_2O_7$, and photocatalytic reaction of Cr(VI) occurred in following way:[S3-S5]

$$H_2CrO_4 + 6H^+ + 3e^- = Cr^{3+} + 4H_2O \quad (1)$$

or

$$HCrO_4^- + 7H^+ + 3e^- = Cr^{3+} + 4H_2O \quad (2)$$

As for alkaline medium, Cr(VI) mainly existed in the form of CrO_4^{2-}, and the reaction proceeded as:

$$CrO_4^{2-} + 4H_2O + 3e^- = Cr(OH)_3 + 5OH^- \quad (3)$$

It was apparent that the acid medium is beneficial to the photocatalytic reduction of Cr(VI) owing to the existence of abundant H^+. Hence, higher reduction efficiency of Cr(VI) would be expected at lower pH. Besides, the photocatalytic efficiency and degradation rate at pH 1 and pH 3 were of little difference. Therefore, various TNRs-C_3N_4-x (x = 0.05, 0.1, 0.2 and 0.5) were evaluated at pH 3.

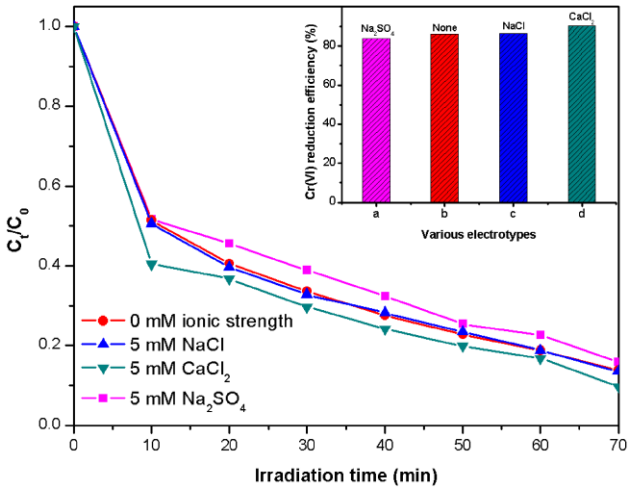

Fig. S6. Photocatalytic reduction of Cr(VI) and removal efficiency (inset) for TNRs-C_3N_4-0.1 when various electrotypes coexisted in reaction systems. Initial concentration of Cr(VI) was at 50 ppm, dosage of TNRs-C_3N_4-0.1 was 1 g L^{-1}, solution pH was 3.0.

Electrolyte effects were examined with NaCl, $CaCl_2$ and Na_2SO_4 at 5 mM, and corresponding removal efficiency of Cr(VI) is presented in Fig. S6. Comparing with the system without any electrolyte, addition of NaCl would not have any effect on photocatalytic reduction of Cr(VI). However, addition of $CaCl_2$ greatly promoted photocatalytic reduction of Cr(VI). On the other hand, addition of Na_2SO_4 inhibits photo-reduction of Cr(VI) primarily due to competitive adsorption of SO_4^{2-} with Cr(VI). Overall, electrolytes had some influence to some extent on the removal efficiencies of Cr(VI).

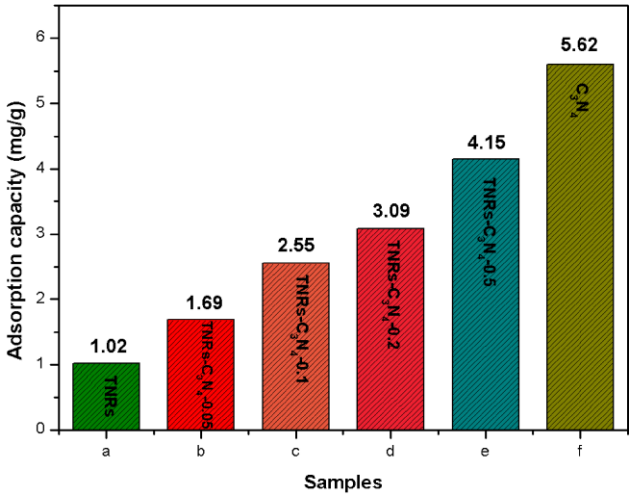

Fig. S7. Adsorption performances of the TNRs, g-C_3N_4, and TNRs-C_3N_4-x (x = 0.05, 0.1, 0.2, and 0.5) for alone RhB solution system. Initial concentration of RhB solution was at 20 ppm, dosage of catalyst was 1 g L^{-1}, and pH of solution was 7.0.

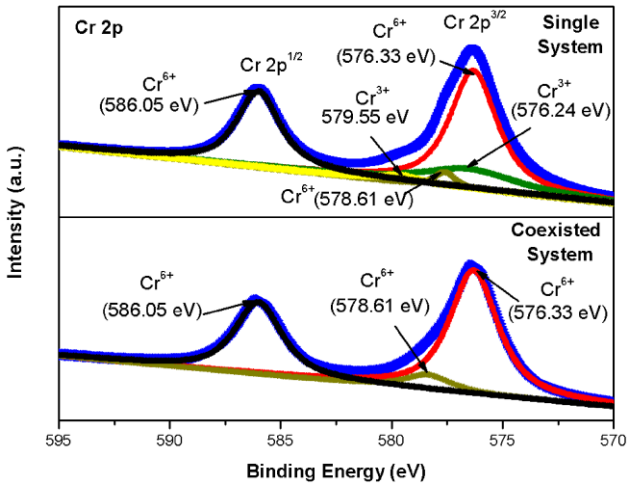

175

176 **Fig. S8.** The XPS spectra of Cr 2p absorbed on the surface of TNRs-C_3N_4-0.1 samples after
177 photocatalytic reaction in the single Cr(VI) system and in the coexisted system of Cr(VI) and
178 RhB.

179

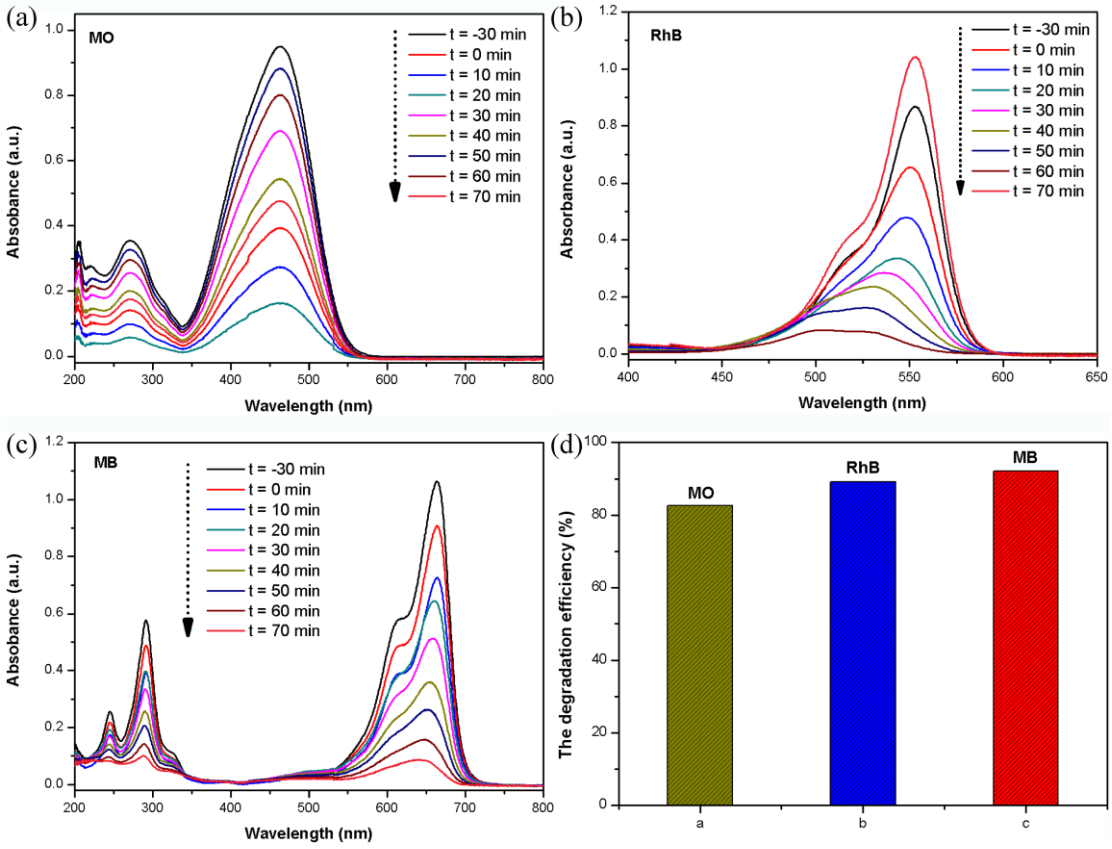

180

181 **Fig. S9.** The photocatalytic degradation and efficiency of TNRs-C_3N_4-0.1 samples for MO, RhB
182 and MB solution, respectively.

183

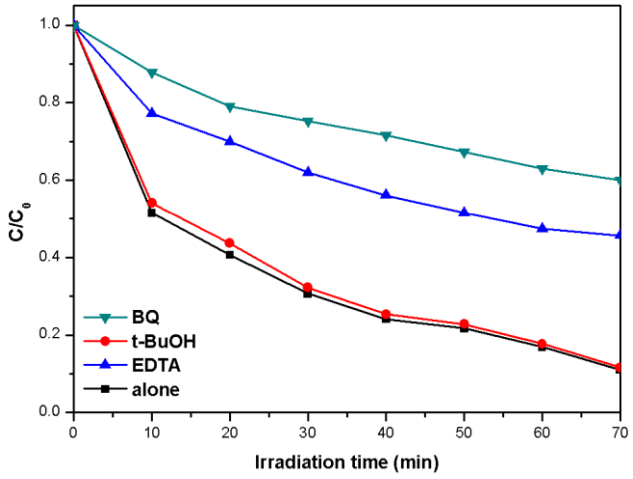

Fig. S10. The comparison of photoactivity toward RhB for TNRs-C_3N_4-0.1 with the addition of BQ, t-BuOH, EDTA, and without scavengers, respectively.

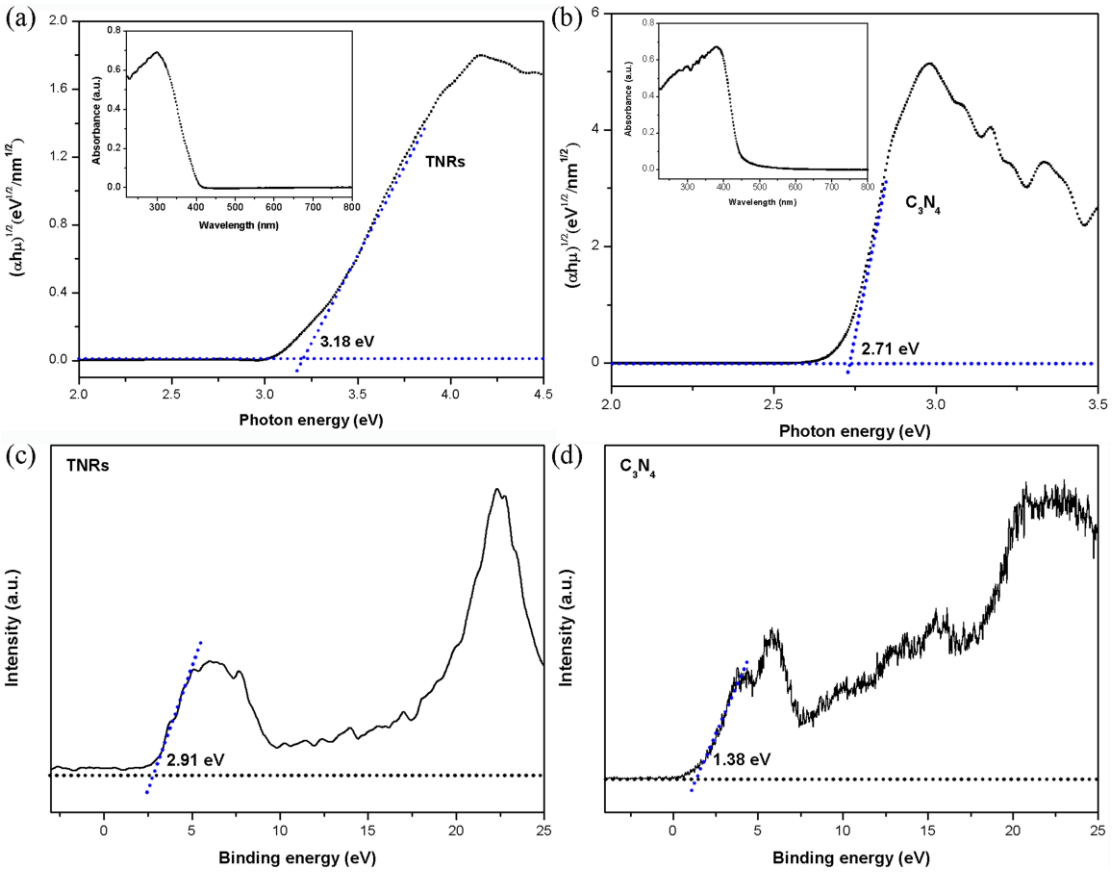

Fig. S11. UV-vis absorption spectra (inset) as well as their related estimation of band gaps of TNRs (a) and g-C_3N_4 (b); Valence-band XPS spectra of TNRs (c) and g-C_3N_4 (d).

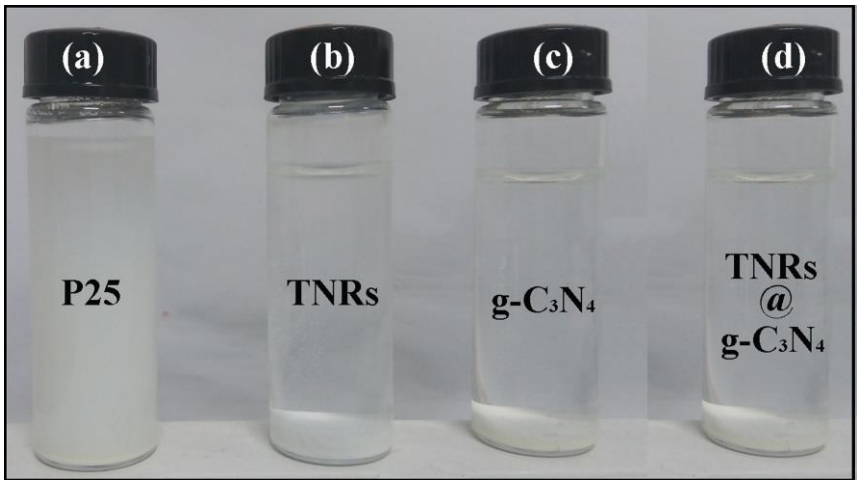

Fig. S12. The appearance of suspensions containing four different types of photocatalysts in water after 1 hour. (a) Degussa P25, (b) TNRs, (c) g-C_3N_4, and (d) TNRs/g-C_3N_4 composites.

References

S1 E. Szabó-Bárdos, E. Pétervári, V. El-Zein, and A. Horváth, *J. Photoch. Photobio. A*, 2006, **184**, 221-227.

S2 D. Lu, P. Fang, X. Liu, S. Zhai, C. Li, X. Zhao, J. Ding, and R. Xiong, *Appl. Catal. B*, 2015, **179**, 558-573.

S3 J.A. Nav, O.G. Colón, M.A. Trillas, J. Peral, X. Domènech, J.J. Testa, J. Padrón, D.Rodr Guez, and M.I. Litter, *Appl. Catal. B*, 1998, **16**, 187-196.

S4 R. Vinu, and G. Madras, *Environ. Sci. Technol.*, 2008, **42**, 913-919.

S5 S. Wang, C. Chen, Y. Tzou, C. Hsu, J. Chen, and C. Lin, *J. Hazard. Mater.*, 2009, **164**, 223-228.

Caption of Figures

Fig. S1. AFM image of as-prepared g-C_3N_4 nanosheets.

Fig. S2. (a) AFM images of pure TiO_2-based nanosheets; (b) line profile showing the height of TiO_2-based nanosheets.

Fig. S3. XPS spectra of C 1s region for TNRs samples (The carbon is derived from carbon contamination for standardizing).

Fig. S4. XPS spectra O 1s region (a) and Ti 2p region (b) of TNRs, TNRs-C_3N_4-0.1, and TNRs-C_3N_4-0.5.

Fig. S5. Photocatalytic reduction of Cr(VI) and the reaction rate constant (A_1) at different pH for TNRs-C_3N_4-0.1 under visible light irradiation. Initial concentration of Cr(VI) was 50 ppm, and the dosage of TNRs-C_3N_4-0.1 was 1 g/L.

Fig. S6. Photocatalytic reduction of Cr(VI) and removal efficiency (inset) for TNRs-C_3N_4-0.1 when various electrotypes coexisted in reaction systems. Initial concentration of Cr(VI) was at 50 ppm, dosage of TNRs-C_3N_4-0.1 was 1 g L^{-1}, solution pH was 3.0.

Fig. S7. Adsorption performances of the TNRs, g-C_3N_4, and TNRs-C_3N_4-x (x = 0.05, 0.1, 0.2, and 0.5) for alone RhB solution system. Initial concentration of RhB solution was at 20 ppm, dosage of catalyst was 1 g L^{-1}, and pH of solution was 7.0.

Fig. S8. The XPS spectra of Cr 2p absorbed on the surface of TNRs-C_3N_4-0.1 samples after photocatalytic reaction in the single Cr(VI) system and in the coexisted system of Cr(VI) and RhB.

Fig. S9. The photocatalytic degradation and efficiency of TNRs-C_3N_4-0.1 samples for MO, RhB and MB solution, respectively.

Fig. S10. The comparison of photoactivity toward RhB for TNRs-C_3N_4-0.1 with the addition of BQ, t-BuOH, EDTA, and without scavengers, respectively.

Fig. S11. UV-vis absorption spectra (inset) as well as their related estimation of band gaps of TNRs (a) and g-C_3N_4 (b); Valence-band XPS spectra of TNRs (c) and g-C_3N_4 (d).

Fig. S12. The appearance of suspensions containing four different types of photocatalysts in water after 1 hour. (a) Degussa P25, (b) TNRs, (c) g-C_3N_4, and (d) TNRs/g-C_3N_4 composites.